Synthesis and tribological studies of nanoparticle additives for pyrolysis bio-oil formulated as a diesel fuel

Xu, Yufu; Peng, Yubin; Zheng, Xiaojing; Dearn, Karl D.; Xu, Hongming; Hu, Xianguo

DOI:
10.1016/j.energy.2015.01.117

Energy 83 (2015) 80–88

Contents lists available at ScienceDirect

Energy

journal homepage: www.elsevier.com/locate/energy

Synthesis and tribological studies of nanoparticle additives for pyrolysis bio-oil formulated as a diesel fuel

Yufu Xu [a, *], Yubin Peng [a], Xiaojing Zheng [b], Karl D. Dearn [c], Hongming Xu [a, c], Xianguo Hu [a]

[a] Institute of Tribology, School of Mechanical and Automotive Engineering, Hefei University of Technology, Hefei 230009, China
[b] School of Arts and Media, Hefei Normal University, Hefei 230601, China
[c] School of Mechanical Engineering, University of Birmingham, Edgbaston, Birmingham B152TT, United Kingdom

ARTICLE INFO

Article history:
Received 8 May 2014
Received in revised form
6 December 2014
Accepted 26 January 2015
Available online 20 March 2015

Keywords:
Lubricity
Nanoparticle
Pyrolysis bio-oil
Alternative fuel
Nano-La_2O_3

ABSTRACT

The tribological behaviour of pyrolysis bio-oil with a synthesized nano-Lanthanum oxide (La_2O_3) additive was evaluated using a point contact four ball tribometer under different frictional conditions. Results were compared against a micro (μ)-La_2O_3 additive and an un-additised bio-oil as a control. The results show that nano-La_2O_3 impregnated bio-oil had better tribological properties than the control groups. Under the operating loads, the optimum nanoparticle concentration within the bio-oil was investigated. At these levels, the combined action of adsorbed bio-oil films on the worn surfaces and the bearing effects of the nano-La_2O_3 minimized friction and wear. The tribo-mechanisms were ascribed to adhesive wear as a result of lubrication starvation under high loads, and abrasive wear at high rotational speeds as a result of combined deformation and aggregation of the nano-La_2O_3 particles.

1. Introduction

Since the energy crisis in 1970s, many countries have focused efforts on the development of alternative sources of energies. In recent decades, bio-oil derived from biomass has been shown as one of the most promising alternatives to the traditional fossil fuels [1–3]. The reasons for this are numerous but include the general availability of the raw materials for the bio-oil that can be derived from waste, and depending on how this is processed there is a potential for the process to be can be carbon neutral. The main components of such bio-oils are oxygen-containing organics including carboxylic acids, alcohols, aldehydes, ketones, phenols etc. Generally, such fuels are prepared though a fast pyrolysis process with the rapid thermal decomposition of biomass in the absence of oxygen at a moderate temperature of ~500 °C at an extremely high heating rate about 400–500 °C/s. As an alternative fuel in internal combustion engines, bio-oil has been shown to enhance combustion characteristics [4]. Bio-oils have also been shown to possess very good lubricating properties. The lubricity of diesel fuels is very important since it has a direct effect on the durability of the fuel injection equipment [5]. Tribologically, some bio-oils have been shown to possess better antifriction properties than those of the conventional fossil fuel. For others however, the wear properties can be much worse, as a result of corrosion and surface degradation. These effects can lead to severe damage of engine components to the extent that the application of bio-oils has been restricted [6–8]. This forms the motivation for seeking methods to upgrade the tribological performance of the bio-oil by inhibiting these negative properties.

Nano-materials exhibit great potential for improving tribological performance and as such they have been widely studied as lubrication additives. Lanthanum oxide is a functional rare earth material and as such, it has found many uses including as a catalyst, and hydrogen storage material [9,10] it also has potential as a tribological additive. For all these applications, the surface shape, particle size, and the dispersed state are of importance. As an example, Xue et al. [11] reported the sliding wear behaviours of nickel composite coatings containing micro- and nano-La_2O_3 particles. They found that the nano-La_2O_3 composite coatings exhibited excellent wear resistance. Nano-La_2O_3 may therefore improve the tribological properties of bio-oil and negate the potential wear limitations outlined above. Furthermore, the use of energetic

* Corresponding author. Tel./fax: +86 551 62901359.
E-mail address: xuyufu@hfut.edu.cn (Y. Xu).

http://dx.doi.org/10.1016/j.energy.2015.01.117

nanoparticles such as La_2O_3, due to small particle size and the relatively low concentration levels, affords a promising method of altering the reactivity of liquid fuels for enhanced combustion stability, resulting in a reduction in ignition delay of some fuels [12].

In this paper, ball-like nano-La_2O_3 was synthesized and dispersed in a pyrolysis bio-oil to form a Bio-Oil/La_2O_3 (BO/La_2O_3) suspension via ultrasonic technology. The effect of La_2O_3 particle size, percentage concentration, friction load and rotational speed on tribological properties were evaluated using a four ball point contact tribometer and the corresponding tribological mechanisms are discussed.

2. Experimental

2.1. Materials

All of the chemicals used in the present work, such as the lanthanum carbonate ($La_2(CO_3)_3$), nitric acid (HNO_3), citric acid monohydrate ($C_6H_8O_7$ H_2O), acetone and the lanthanum oxide (micro-La_2O_3), were analytical grade reagents.

The BO used was from rice husk via fast pyrolysis technology and was provided by Anhui Province Key Laboratory of Biomass Clean Energy, University of Science and Technology of China. The components of bio-oil were as follows: carboxylic acids 32.72%; alcohols 8.14%; aldehydes 23.49%; ketone 7.09%; phenols 13.98%, and others 14.58%. The main physicochemical properties are as follows: The flash point is 68 °C; high heating value is 16.5 MJ/kg; kinematic viscosity is 13.2 $mm^2\ s^{-1}$ at 40 °C. It should be noted that although the low heating value and high viscosity of the bio-oil in its present form make it unsuitable for use a fuel, upgrading via emulsification would rectify this. More details of the pyrolysis process, chemical composition and physicochemical properties can be found elsewhere [13].

2.2. Preparation of nano-La_2O_3

The preparation of the *nano-La_2O_3* comprised the following steps. 25 mmol of $La_2(CO_3)_3$ (~11.4 g) and 150 mmol of HNO_3 (~9.4 ml) were dissolved into 100 ml of distilled water to form a clear reaction solution. This was then heated at 60 °C for 5 min after which 8.3 mmol of $C_6H_8O_7{\cdot}H_2O$ (~1.74 g) was added to it, and magnetically stirred to form a uniform dispersion. This was then heated in a muffle furnace to remove excess water, allowing a gel to form. The precursor was then dried and the nano-La_2O_3 (nano lanthanum oxide) was produced via calcination at 850 °C for 6 h [14]. Finally the La_2O_3 was added to bio-oil at concentration levels of 0.2, 0.6, 1.0, 1.4 and 1.8% (all the % in this paper means wt.%). Each BO/La_2O_3 suspension was stable for at least 7 days after being ultrasonically dispersed for 10 min before each test.

2.3. Tribological tests

The tribological tests were carried out on a Jinan MQ-800 four-ball tribometer. The schematic of the tribological tests is shown in Fig. 1. Referring to ASTM D4172 (Standard Test Method for Wear Preventive Characteristics of Lubricating Fluid), the experimental conditions selected were nominally a load of 100 N with a rotational speed of 1250 rpm at 25 ± 2 °C for 30 min. ASTM E52100 bearing steel test samples were used with a diameter of 12.7 mm, a surface roughness (Ra) of 0.032 μm and a hardness of 61–63 HRC. Experiments were compared against a control sample comprising the bio-oil without additives. These experimental conditions ensured that all of the tribological tests were performed under the boundary lubrication.

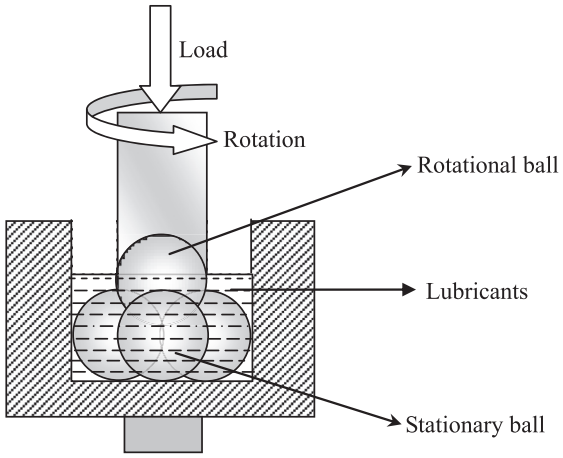

Fig. 1. Schematic of the tribological tests.

After each test, the steel balls were washed using acetone. Wear rates were was evaluated from the average WSD (wear scar diameter) of the three lower specimens. After an initial test programme, the effects of load and speed for the bio-oil with nano-La_2O_3 were also evaluated, at 150 N and 200 N and 1450 and 1650 rpm, respectively. Test conditions were repeated three times and the friction coefficient was collected in real-time during each experiment.

2.4. Characterization

The particle size distribution of the La_2O_3 powder was measured using a Bettersize BT-9300H laser particle size analyser. The crystal structure of the precipitate was analysed with a Rigaku D/Max-cB powder XRD (X-ray diffractometer) with Cu Kα radiation (γ = 0.541 nm) under 40 kV, 100 mA and a scanning speed of 5° min^{-1}. The topography of the particles and elemental composition of the worn surfaces was observed using a FEI Sirion 200 SEM (scanning electron microscope) with EDS (energy dispersive spectroscopy). The morphologies and chemical valences of elements on the worn surfaces were analysed using an Olympus TPF-1 optical microscope and a Thermo Scientific ESCALAB 250 XPS (X-ray photoelectron spectroscope), respectively. The WSD of the lower specimens was measured with an accuracy of 0.01 mm. In order to analyse the tribological mechanisms, the thickness of lubricating oil film was calculated with the following formula [15]:

$$\frac{h_{mean}}{R} = 2.69\left(\frac{U\eta_0}{ER}\right)^{0.67}(\alpha E)^{0.53}\left(\frac{W}{ER^2}\right)^{-0.067}\left(1-0.61e^{-0.73k}\right)$$

where h_{mean} is the mean oil film thickness; η_0 is the viscosity of the lubricant; R is the radius of curvature; U is the entraining surface velocity; E is Young's modulus (E = 210 GPa); α is the Pressure-viscosity coefficient, ($\alpha = 0.44 \times 10^{-8}$ m^2/N pa^{-1}); W is the contact load and k is the ellipticity parameter, k = 1.03.

3. Results and discussion

3.1. Characterization of the La_2O_3

Fig. 2 shows the variation in the surface morphologies of micro (μ) and nano-La_2O_3 particles. The μ-La_2O_3 is generally rod-like with particle diameters of between approximately 1.0–4.0 μm with a median diameter (D50) of 2.6 μm. However, the nano-La_2O_3 is quite different, displaying ball-like particles, with diameters of

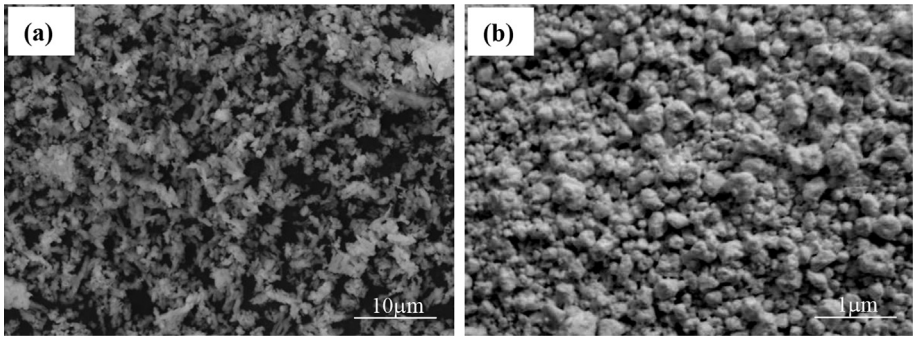

Fig. 2. SEM images of (a) μ-La_2O_3, and (b) nano-La_2O_3.

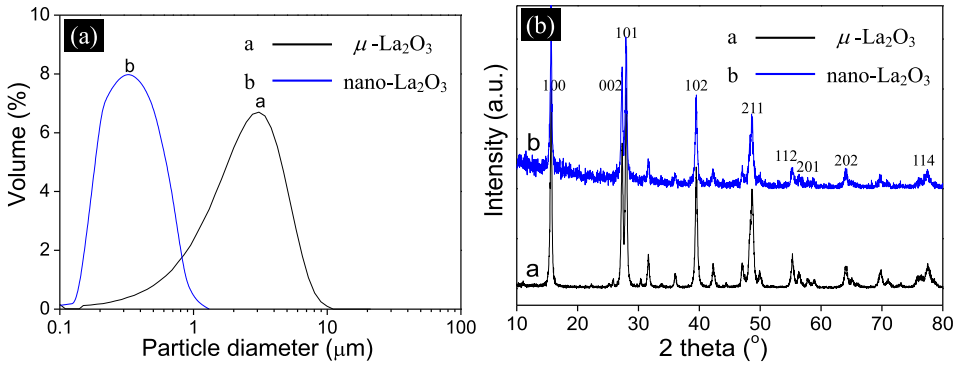

Fig. 3. The particle size distribution (a) and XRD patterns (b) of La_2O_3.

approximately 20–1000 nm. The particle size distributions of the La_2O_3 are shown in Fig. 3a. It should be noted that the sizes of La_2O_3 shown in Fig. 3a are smaller and more uniformly dispersed than in Fig. 2. This discrepancy is caused by the different test methods employed. The solid powders used in the SEM analysis were prone to agglomeration [16], but for the laser particle size analysis the powder was dispersed in circulating water.

The XRD pattern of the μ-La_2O_3 and nano-La_2O_3 is shown in Fig. 3b. The main diffraction peaks can be indexed as La_2O_3 (JCPDS No. 41-4019), and the intense narrow peaks show that both of the La_2O_3 samples were highly crystalline. This can be further verified according to Scherrer's formula [17]:

$$D_{h,k,l} = K\lambda/(\beta\cos\theta)$$

where, D is the average crystallite diameter, K is a dimensionless shape factor and was taken as 0.89, λ is the X-ray wave length which in this case was 0.15418 nm, β is the half maximum line width, and θ is the Bragg angle,

The average crystallite diameters calculated using Scherer's equation were consistent with the XRD spectra, indicating that the synthesis of the nano-La_2O_3 was successful.

3.2. *Effect of additive particle size on the friction and wear properties of bio-oil*

Fig. 4 shows the variation of WSD (a) and average friction coefficient (b) with increasing content of the micro and nano BO/La_2O_3 at a load of 100 N and a rotational speed of 1250 rpm. There were differences between the observed friction and wear properties of the oils with micro and nano La_2O_3 particles. For the μ-La_2O_3, the WSD below concentrations of 0.6% was steady. Beyond this level, wear increases rapidly with a rise in La_2O_3 from 1% to 1.8%. This may be due to increasing levels of La_2O_3, leading to the

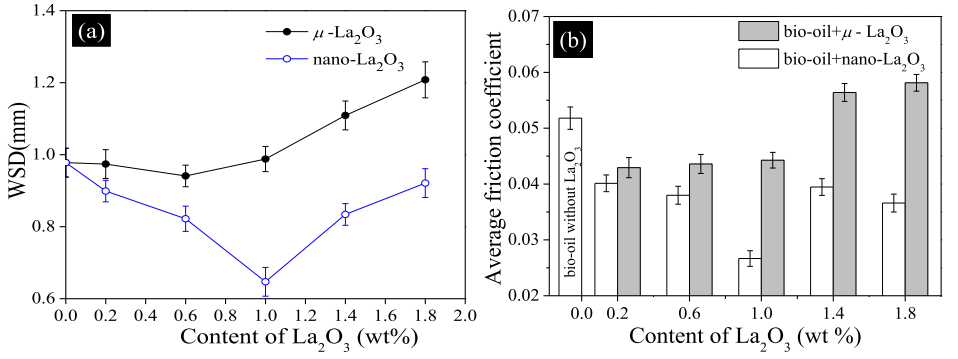

Fig. 4. Variation of WSD (a) and average friction coefficients (b) with increasing content of La_2O_3 in bio-oil (100 N, 1250 rpm for 30 min).

formation of bio-oil films with solid particles combined with the particle geometry. It is likely that the cylindrical shape of the μ-La_2O_3 particles resulted in abrasive wear at the contact interface similarly to the effects reported in Refs. [18,19].

Trends for the nano-La_2O_3 indicate that it had a better wear resistance than the micro additive and in all cases improved the tribological properties compared to bio-oil without additives. The WSD decreased as the blended ratios increased to 1%. Beyond this concentration, wear damage steadily increased. This behaviour could be explained by considering again the geometry of the additive particles. Up to 0.6%, the ball-like nano-La_2O_3 may have acted as a bearing between the surfaces, sustaining and distributing contact loads. The measured particle sizes of the nano-La_2O_3 were of a similar magnitude to the surface roughness of the contact interface (32 nm) which could also have contributed to this [20]. Beyond 1% concentrations, the nano-La_2O_3 was shown to

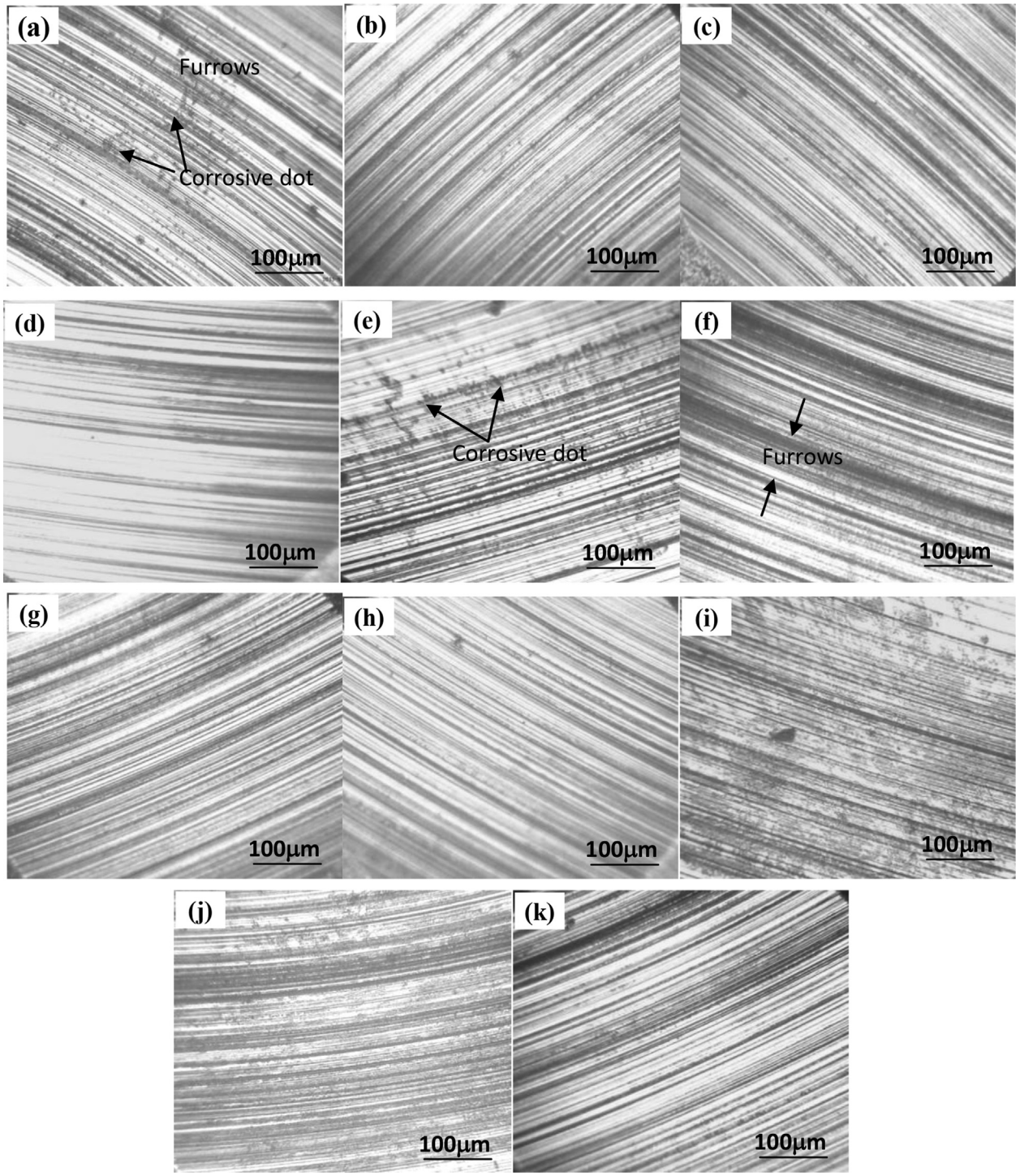

Fig. 5. Optical micrographs of worn surfaces of upper balls specimens lubricated with bio-oil containing (a) no La_2O_3, (b) 0.2% μ-La_2O_3, (c) 0.6% μ-La_2O_3, (d) 1% μ-La_2O_3, (e) 1.4% μ-La_2O_3, (f) 1.8% μ-La_2O_3, (g) 0.2% nano-La_2O_3, (h) 0.6% nano-La_2O_3, (i) 1% nano-La_2O_3, (j) 1.4% nano-La_2O_3, and (k) 1.8% nano-La_2O_3 (100 N, 1250 rpm for 30 min).

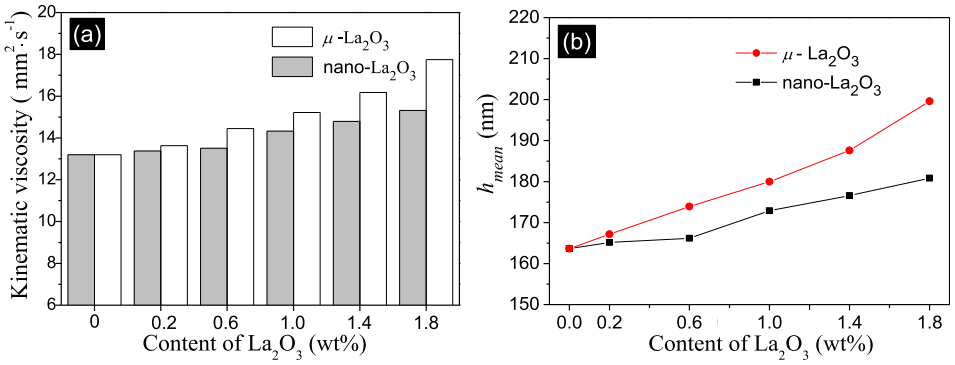

Fig. 6. Variation of (a) kinematic viscosity and (b) mean oil film thickness (h_{mean}) for bio-oils with increasing contents of μ-La_2O_3 and nano-La_2O_3 (100 N, 1250 rpm for 30 min).

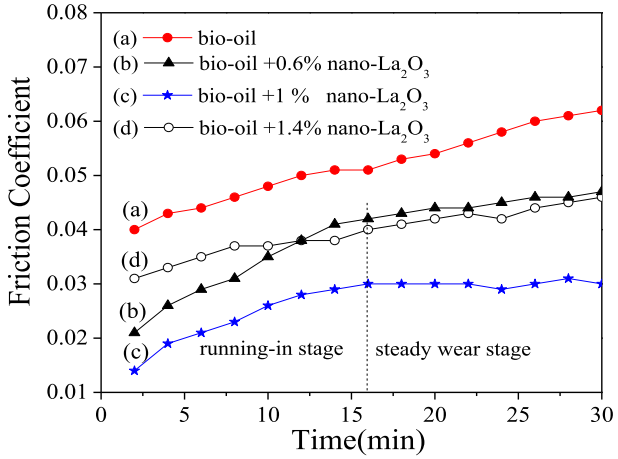

Fig. 7. Variation of friction coefficients against time when lubricated with bio-oil containing different concentrations of nano-La_2O_3 (1250 rpm and 100 N for 30 min).

agglomerate into larger clusters thus weakened the effect described above leading to an increased WSD. The frictional characteristics displayed similar behavioural trends. The results shown in Fig. 4 suggested an optimal nano-La_2O_3 blend ratio (i.e. when the tribological properties were at their best) occurred at a concentration of 1% in the bio-oil.

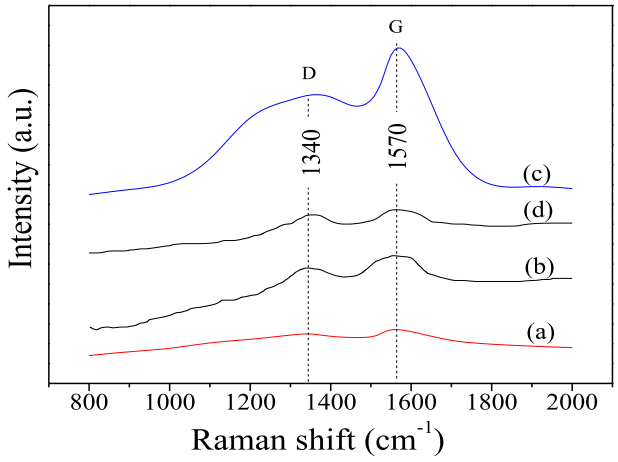

Fig. 8. Raman spectra of worn surfaces lubricated with bio-oil (a), bio-oil + 0.6% nano-La_2O_3 (b), bio-oil + 1% nano-La_2O_3(c), and bio-oil + 1.4% nano-La_2O_3 (d) (1250 rpm and 100 N for 30 min).

The optical micrographs of the worn surfaces taken from the upper specimens are shown in Fig. 5. The worn surface of the control sample (Fig. 5a) displayed evidence of corrosive damage and many wide and deep furrows. The corrosion seen on the contact surface was a result of acidic components within the bio-oil (such as acetic and formic acid) [6]. For the μ-La_2O_3 concentrations of between 0.2 and 1% did not show any evidence of corrosion (Fig. 5b–d). The corrosion phenomena are likely to have been avoided by the La_2O_3 particles adsorbing the acidic components of the biofuel, aided by the high specific surface area of the particles [10]. However, the corrosive damage returned when μ-La_2O_3 content was increased above 1% (Fig. 5e–f). These observations are consistent with the tribological behaviour described above. When the concentration of μ-La_2O_3 is no more than 1%, the cylindrical shaped particles can roll in plane preventing contact between surfaces and reducing chemical attack. However, adsorption of the acidic components from the bio-oil by the μ-La_2O_3 (above 1%) led to further agglomeration and then larger particle abrasive damage at the contact interface. The freshly abraded surfaces were then more likely to be susceptible to further corrosion followed by wear etc., a cycle similar to that described in Ref. [21].

The evidence of wear and surface damage was much less for the nano-La_2O_3 experiments as can be seen in Fig. 5g–i. At concentration levels up to 1%, furrows on the worn surfaces were shallow and this may be due to the topography of the nano particles. Surface damage and wear increased (Fig. 5j, k) when content exceeded 1% and was most likely due to the aggregation of the nano-additives. This is an effect that has been described in Ref. [22]. Consequently, the nano-La_2O_3 displayed optimal antifriction and antiwear properties at a weight content of 1% in the bio-oil.

The kinematic viscosity and average oil film thicknesses are shown in Fig. 6, whereas the concentration of La_2O_3 is shown to have increased, so too does the kinematic viscosity and oil film thickness. The μ-La_2O_3 was calculated to have formed thicker oil films between the frictional surfaces than the nano-La_2O_3. This was likely to have been caused by the larger particle diameters of the μ-La_2O_3 which led to a higher viscosity for the respective bio-oil blends. Despite this, the friction coefficient and wear volume of the steel specimens was considerably higher than the nano-La_2O_3. The reason for this is that the peak oil film thickness was calculated to be approximately 200 nm, however the average measured diameter of the μ-La_2O_3 particles was at least several micrometres. It is assume therefore, that the μ-La_2O_3 in the bio-oil acted as a form of abrasive debris leading to high wear. Conversely, the average diameter of the nano-La_2O_3 particles was well below the calculated film thicknesses. This theory holds up to concentrations of 1%. Beyond this point, aggregation of the nano particles (leading to the formation of micron-sized debris) had a negative effect on the

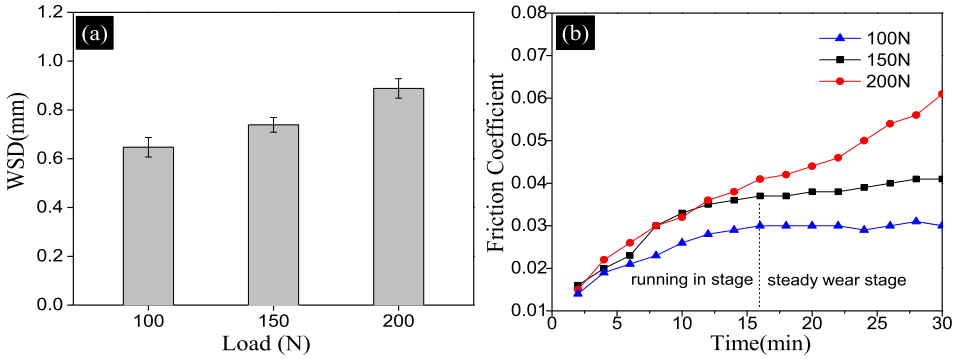

Fig. 9. Variation of WSD (a), and friction coefficient–time curves (b) with load (1% nano-La_2O_3, 1250 rpm for 30 min).

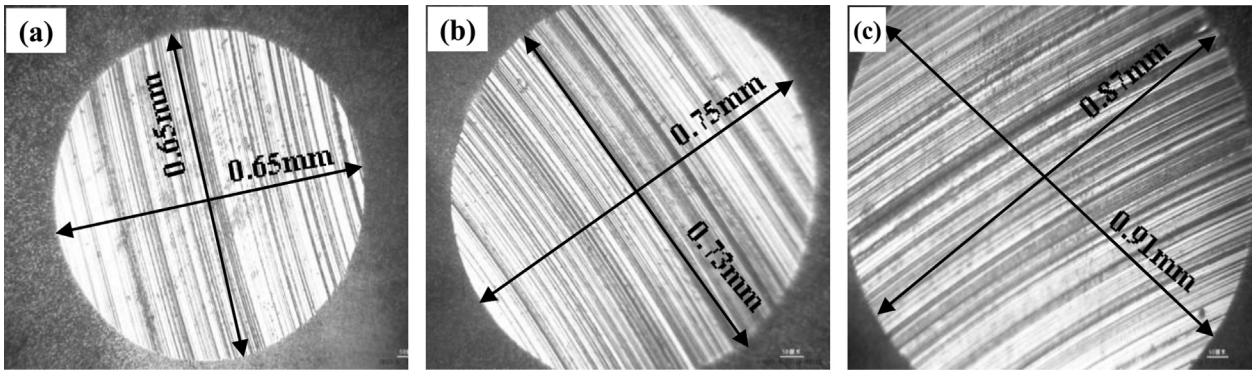

Fig. 10. Optical micrographs of worn surfaces of lower specimens under (a) 100 N, (b)150 N, and (c) 200 N (1% nano-La_2O_3, 1250 rpm for 30 min).

tribological properties of the bio-oil suspensions. This was despite the film thickness continuing to increase.

The results given in Figs. 2–6 overwhelmingly show that the nano-La_2O_3 impregnated BO had a better tribological performance than those of μ-La_2O_3, therefore, the following sections focus solely on the performance of the nano-La_2O_3 dispersed bio-oil.

Fig. 7 shows variation of friction coefficients against time with test specimens subjected to a 100 N load, rotating at 1250 rpm for 30 min. The friction coefficient of control sample is the highest of the observed fuels with no clear indication of the transition between running-in and steady state conditions. This may be due to the corrosive action of the acidic components within the bio-oil [13]. However, there are clear transitions between initial and steady state conditions for the nano-La_2O_3 bio-oils The transient friction coefficients of the bio-oils containing 0.6% and 1.4% nano-La_2O_3 particles are similar. Variations between these two oils can be attributed to the role of aggregation of the nano particles (first forming and then dispersing similar to phenomenon described in Ref. [23]). The equilibrium point for the optimized lubricity occurs at a content of 1% nano-La_2O_3.

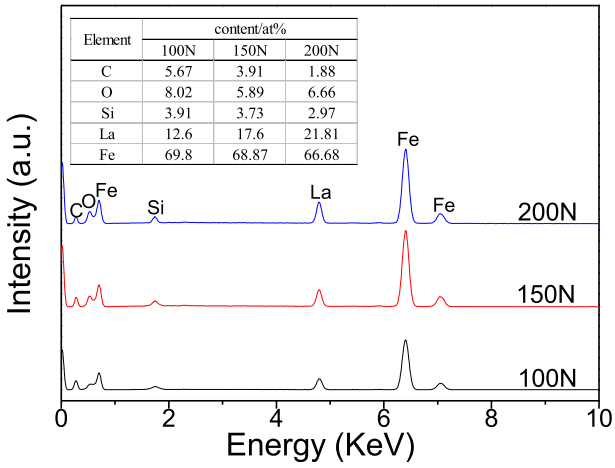

Fig. 11. EDS spectra of the worn surfaces that have transmitted (a) 100 N, (b)150 N, and (c) 200 N (1% nano-La_2O_3, 1250 rpm for 30 min).

Fig. 8 shows the Raman spectra of the worn surfaces of the test specimens. Two typical characteristic peaks at the D and G bands, located at 1340 cm^{-1} and 1570 cm^{-1}, respectively can clearly be seen. Both of these two peaks were very weak without the additive, however, in the strength grew as the concentration of nano-La_2O_3 in the bio-oil increased. This indicated that the transmission (i.e. the rolling and compressive action) of the La_2O_3 through the contact may have contributed to the adsorption, onto the frictional surfaces, of organics from the bio-oil, leading to a reduction in friction. At higher concentration levels, this effect was countered by the increased aggregation of nano-La_2O_3 particles (e.g. at 1.4%). These results are in agreement with the trends seen in Fig. 6.

3.3. *Effects of load on the friction and wear properties of the bio-oil with nano-additives*

Fig. 9 shows the variation of WSD and transient friction coefficient with varying loads for 1% nano-La_2O_3 bio-oil at 1250 rpm for 30 min. Both were shown to increase with the increasing load. However neither relationship was linear as the higher loads prohibited the transition from mild to severe wear by increasing the real area of contact [24]. With the increase of the load, the oil film

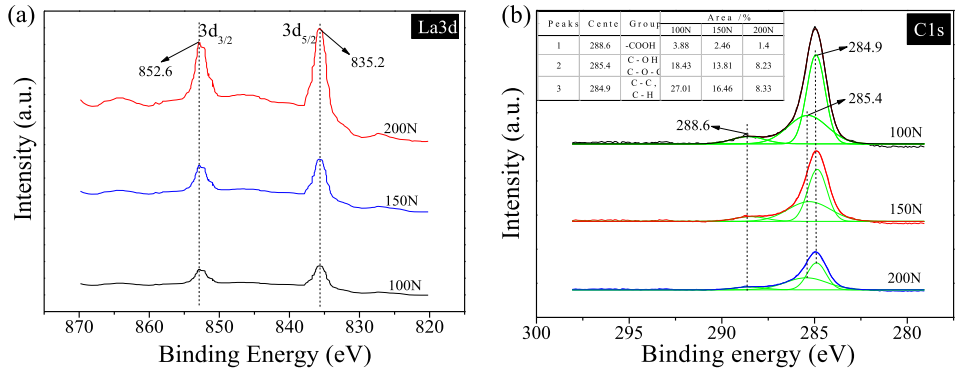

Fig. 12. XPS spectra of typical elements La3d (a) and C1s (b) on the worn surfaces that have transmitted 100 N, 150 N, and 200 N (1% nano-La_2O_3, 1250 rpm for 30 min).

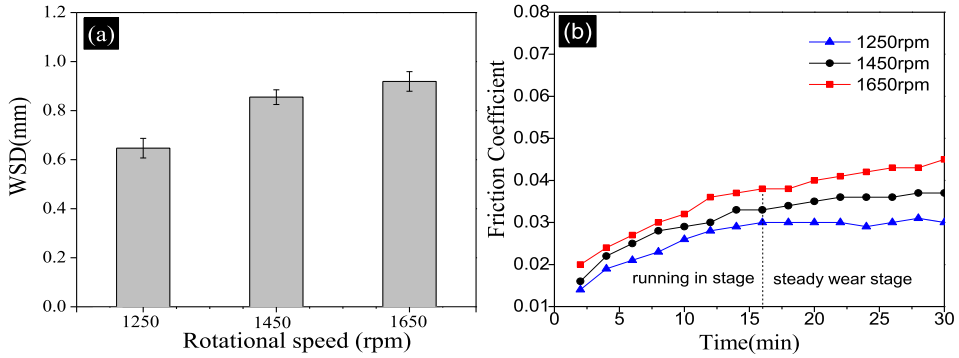

Fig. 13. Variation of WSD (a), and friction coefficient–time curves (b) with rotational speed (1% nano-La_2O_3, 100 N for 30 min).

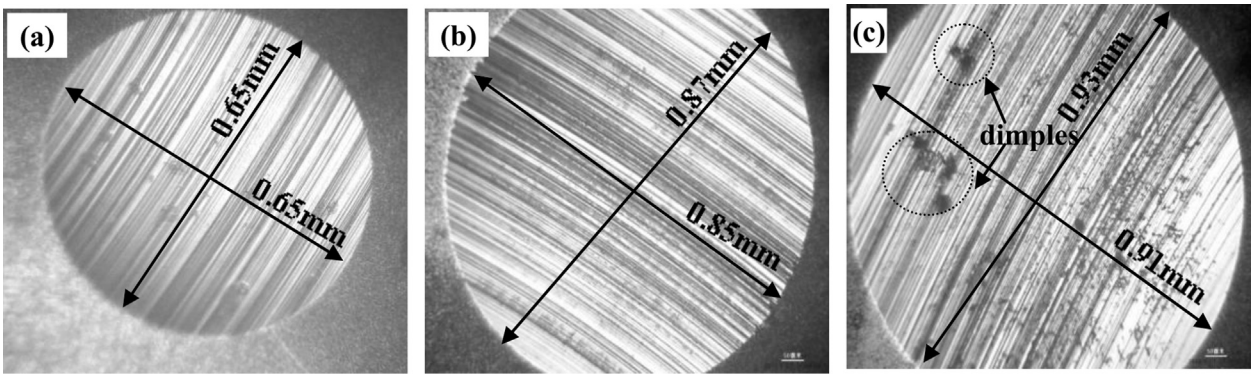

Fig. 14. Optical micrographs of the worn surfaces of lower specimens under (a) 1250 rpm, (b) 1450 rpm, and (c) 1650 rpm (1% nano-La_2O_3, 100 N for 30 min).

formed and adsorbed between the worn surfaces were also easier to break down [25]. Increasing the load would also have affected the beneficial effect of the geometry of the nano-La_2O_3 by causing deformation of the ball-like load bearing particles. These are likely to be the root causes of the increasing friction coefficient with load. These effects may also be contributing factors to the lack of a transitional point between the transient and steady state conditions at the highest load. This may indicate the load limit for the nano-La_2O_3.

Fig. 10 shows the surface topography of the lower specimens for the various loads (100 N, 150 N, and 200 N) displays the extent of surface damage and wear. The transmission of higher normal loads was likely to prevent the formation, at the contact interface, of robust lubricating oil films, leading to oil starvation and adhesive wear [26,27].

Fig. 11 shows the EDS spectra from the worn surfaces (shown in Fig. 10.). An increase in the loads carried by the specimens, led to both an increase in the deposition at the surface of elemental Lanthanum and a reduction in carbon. These elemental characteristics suggested that though the nano-La_2O_3 carried part of the load transmitted through the surfaces, an increased loading, significantly reduced the effectiveness of the protective oil film. The combined effect of which was an increased friction and wear profile.

The XPS spectra for the same surfaces are shown in Fig. 12. The peaks at 852.6 eV and 835.2 eV can be ascribed to La3$d_{3/2}$ and La3$d_{5/2}$ of La3d, respectively, suggesting that Lanthanum on the worn surfaces emanated from the La_2O_3. In addition to these, the peaks at 288.6 eV, 285.4 eV and 284.9 eV were ascribed to the –COOH, C–OH(C–O–C), and C–C(C–H) groups, respectively. These

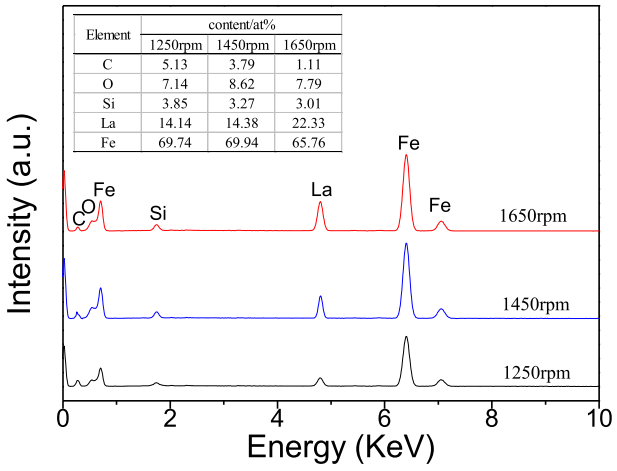

Fig. 15. EDS spectra of the worn surfaces lubricated with bio-oil containing 1% nano-La_2O_3 under different rotating speed (Load: 100 N for 30 min).

functional groups will have been derived from the acids, alcohols, and carbon chains in the bio-oil. Another effect of increasing the load was reduction in the area of all the observed peaks (and hence a drop in the chemical contents on the surface). This provides confirmation that the most active wear mechanism was adhesive wear, caused by oil starvation between the specimens.

3.4. Effects of rotational speed on the friction and wear properties of the bio-oil with nano-additives

The following tests were conducted with bio-oil containing 1% nano-La_2O_3 under 100 N for 30 min. Fig. 13 shows a weak correlation between the WSD and friction coefficient with rotational speed. The friction coefficient increased accordingly with speed from 1250 rpm to 1650 rpm. This was caused by the combined action of the nano-La_2O_3 and the many organics within the polar groups in the bio-oil [28]. These polar groups are adsorbed on to the contact surfaces leading to good frictional properties. These are further enhanced by the bearing effect derived from the ball-like nano-La_2O_3 particles. The increased rotational speed hindered the adsorption of these polar groups [29] leading to accelerated deformation of the nano-La_2O_3. The aggregated and deformed nano-La_2O_3 becomes abrasive debris. As a result of this, the friction coefficient increases.

The optical micrographs of the worn surfaces of the lower specimens from the rotational speed tests are shown in Fig. 14. These again display very similar characteristics to those already described above (from Figs. 9a and 10a) which also serves to confirm the experimental reliability. The diameter and deformation of wear scar increased with speed. The dimples observed at the highest rotational speed (Fig. 10c), may have been due to a ploughing effect induced by the deformed La_2O_3 as abrasive particles [30].

Fig. 15 shows the EDS spectra of the same worn surfaces. The elemental patterns indicate that carbon is reduced on the worn surfaces whilst elemental Lanthanum increases. Increasing the rotational speed contributed to the deposition of nano-La_2O_3 on to the surfaces but would also have been unfavourable for the deposition of organics. The XPS spectra shown in Fig. 16 provide an explanation of the source of the Lanthanum detected on the worn surface. This indicated that it was derived from the La_2O_3 additive and that the La deposit increased with speed. However, the residue from the tribo-film created by the bio-oil was significantly reduced, which is in agreement with the results presented above.

4. Conclusions

This paper has described a study of the tribological properties of bio-oil enhanced with a La_2O_3 suspension. Rotational speed, normal load, particle size (micro and nano particles) and concentration (between 0 and 2%) of synthesized La_2O_3 were assessed using a MQ-800 four-ball tribometer. Tribological behaviour was fully characterized using a range of observational, numerical and chemical analysis techniques. The following conclusions can be drawn from this study:

a. The nano-La_2O_3 had better antifriction and antiwear properties than those of μ-La_2O_3 as a lubricating additive of bio-oil. For μ-La_2O_3, when its content in bio-oil was less than 1%, there was little effect on wear and a minor influence on anti-frictional properties. When the concentration exceeded 1%, the particles tended to aggregate and act as an abrasive between the contact surfaces. For the nano-La_2O_3, both the wear and friction coefficient first decreased and then increase with La_2O_3 concentration, the optimal weight content seemed to be 1%.
b. The introduction of nano-La_2O_3 reduced corrosive wear, sometimes prevalent in of the bio-oil and derived from the acidic components within the fuel. It also provided a stable foundation for transient friction properties with a clear and distinct transition between running-in and steady state conditions.
c. For bio-oil containing 1% nano-La_2O_3, wear and friction coefficient increased with load and speed. However, the specific wear rate decreased and steady state conditions prevailed under the highest loads and rotational speeds. This was indicative of an

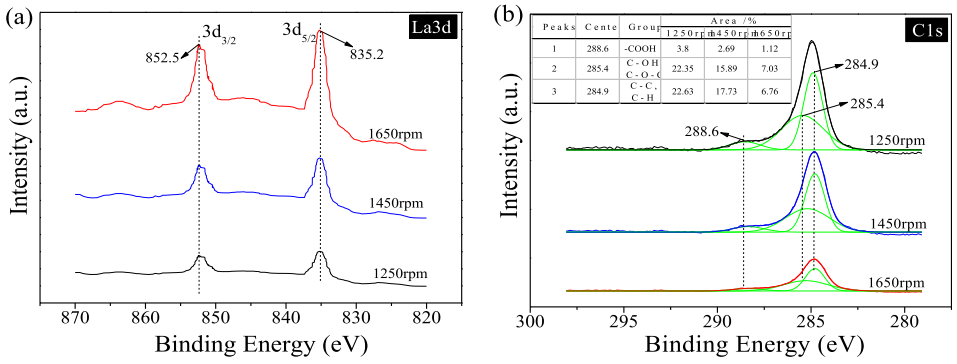

Fig. 16. XPS spectra of typical elements La3d (a) and C1s (b) on the worn surfaces under 1250 rpm, 1450 rpm, and 1650 rpm (1% nano-La_2O_3, 100 N for 30 min).

excellent lubrication performance for the bio-oil containing 1% nano-La_2O_3 for all of the frictional conditions simulated.

d. The tribological mechanisms for the nano-La_2O_3 could be attributed to a combined action between the oil films from bio-oil being adsorbed on to the contact surfaces and a bearing effect from the ball-like nano-La_2O_3 particles. Adhesive wear due to lubrication starvation throughout the contact was the predominant wear mechanism under high loads. At high rotational speeds, abrasive wear became the principal mechanism of wear, as a result of agglomeration and deformation of nano-La_2O_3 particles.

Acknowledgements

The financial support from the National Natural Science Foundation of China (Grant no. 51405124), the Research Fund for International Young Scientists of NSFC (Grant no. 51450110436), China Postdoctoral Science Foundation (Grant no. 2014M560505), Anhui Provincial Natural Science Foundation (Grant no. 1408085ME82) and EPSRC Project (Grant no. EP/J00930X/1) are gratefully acknowledged.

References

[1] Ki OL, Kurniawan A, Lin CX, Ju Y-H, Ismadji S. Bio-oil from cassava peel: a potential renewable energy source. Bioresour Technol 2013;145:157–61.
[2] Capunitan JA, Capareda SC. Characterization and separation of corn stover bio-oil by fractional distillation. Fuel 2013;112:60–73.
[3] Xu Y, Zheng X, Yin Y, Huang J, Hu X. Comparison and analysis of the influence of test conditions on the tribological properties of emulsified bio-oil. Tribol Lett 2014;55:543–52.
[4] Yang SI, Hsu TC, Wu CY, Chen KH, Hsu YL, Li YH. Application of biomass fast pyrolysis part II: the effects that bio-pyrolysis oil has on the performance of diesel engines. Energy 2014;66:172–80.
[5] Sukjit E, Dearn KD. Enhancing the lubricity of an environmentally friendly Swedish diesel fuel MK1. Wear 2011;271(9–10):1772–7.
[6] Xu Y, Wang Q, Hu X, Li C, Zhu X. Characterization of the lubricity of bio-oil/diesel fuel blends by high frequency reciprocating test rig. Energy 2010;35(1):283–7.
[7] Hu E, Xu Y, Hu X, Pan L, Jiang S. Corrosion behaviors of metals in biodiesel from rapeseed oil and methanol. Renew Energ 2012;37:371–8.
[8] Yang Y, Brammer JG, Ouadi M, Samanya J, Hornung A, Xu HM, et al. Characterisation of waste derived intermediate pyrolysis oils for use as diesel engine fuels. Fuel 2013;103:247–57.
[9] Neumann A, Walter D. The thermal transformation from lanthanum hydroxide to lanthanum hydroxide oxide. Thermochim Acta 2006;445(2):200–4.
[10] Wang G, Zhou Y, Evans DG, Lin Y. Preparation of highly dispersed nano-La_2O_3 particles using modified carbon black as an agglomeration inhibitor. Ind Eng Chem Res 2012;51(45):14692–9.
[11] Xue Y-J, Li J-S, Ma W, Zhou Y-W, Duan M-D. Sliding wear behaviors of electrodeposited nickel composite coatings containing micrometer and nanometer La_2O_3 particles. J Mater Sci 2006;41(6):1781–4.
[12] Allen C, Mittal G, Sung C-J, Toulson E, Lee T. An aerosol rapid compression machine for studying energetic-nanoparticle-enhanced combustion of liquid fuels. P Combust Inst 2011;33(2):3367–74.
[13] Lu Q, Yang XL, Zhu XF. Analysis on chemical and physical properties of bio-oil pyrolyzed from rice husk. Anal Appl Pyrol 2008;82:191–8.
[14] Arumugam D, Paruthimal Kalaignan G. Synthesis and electrochemical characterizations of nano-La_2O_3-coated nanostructure $LiMn_2O_4$ cathode materials for rechargeable lithium batteries. Mater Res Bull 2010;45(12):1825–31.
[15] Hu E, Hu X, Liu T, Fang L, Dearn KD, Xu H. The role of soot particles in the tribological behavior of engine lubricating oils. Wear 2013;304(1–2):152–61.
[16] Zook JM, Rastogi V, MacCuspie RI, Keene AM, Fagan J. Measuring agglomerate size distribution and dependence of localized surface plasmon resonance absorbance on gold nanoparticle agglomerate size using analytical ultracentrifugation. ACS Nano 2011;5(10):8070–9.
[17] Hu KH, Liu M, Wang QJ, Xu YF, Schraube S, Hu XG. Tribological properties of molybdenum disulfide nanosheets by monolayer restacking process as additive in liquid paraffin. Tribol Int 2009;42(1):33–9.
[18] Petrica M, Badisch E, Peinsitt T. Abrasive wear mechanisms and their relation to rock properties. Wear 2013;308(1–2):86–94.
[19] Stachowiak GP, Podsiadlo P, Stachowiak GW. Shape and texture features in the automated classification of adhesive and abrasive wear particles. Tribol Lett 2006;24(1):15–26.
[20] Tahamtan S, Emamy M, Halvaee A. Effects of morphological characteristics of alumina particles and interfacial bonding strength on wear behavior of nano/micro-alumina particulates reinforced Al/A206 matrix composites. Tribol Lett 2013;51(3):499–511.
[21] Akonko S, Li DY, Ziomek-Moroz M. Effects of cathodic protection on corrosive wear of 304 stainless steel. Tribol Lett 2005;18(3):405–10.
[22] di Stasio S, LeGarrec JL, Mitchell JBA. Synchrotron radiation studies of additives in combustion, II: soot agglomerate microstructure change by alkali and alkaline-earth metal addition to a partially premixed flame. Energy Fuel 2011;25(3):916–25.
[23] Kalin M, Kogovšek J, Remškar M. Mechanisms and improvements in the friction and wear behavior using MoS_2 nanotubes as potential oil additives. Wear 2012;280–281(0):36–45.
[24] Hiratsuka Ki, Inagaki M. Effects of temperature, sliding velocity and non-friction time on severe-mild wear transition of iron. Tribol Int 2012;49:39–43.
[25] Quinchia LA, Delgado MA, Reddyhoff T, Gallegos C, Spikes HA. Tribological studies of potential vegetable oil-based lubricants containing environmentally friendly viscosity modifiers. Tribol Int 2014;69:110–7.
[26] Prakash B, Hiratsuka Ki. Sliding wear behaviour of some Fe-, Co- and Ni-based metallic glasses during rubbing against bearing steel. Tribol Lett 2000;8(2–3):153–60.
[27] Dearn KD, Hoskins TJ, Petrov DG, Reynolds SC, Banks R. Applications of dry film lubricants for polymer gears. Wear 2013;298–299:99–108.
[28] Xiong W-M, Zhu M-Z, Deng L, Fu Y, Guo Q-X. Esterification of organic acid in bio-oil using acidic ionic liquid catalysts. Energy Fuel 2009;23(4):2278–83.
[29] Jiménez AE, Bermúdez MD, Carrión FJ, Martínez-Nicolás G. Room temperature ionic liquids as lubricant additives in steel–aluminium contacts: influence of sliding velocity, normal load and temperature. Wear 2006;261(3–4):347–59.
[30] Sahoo R, Mantry S, Sahoo TK, Mishra S, Jha BB. Effect of microstructural variation on erosion wear behavior of Ti-6Al-4V alloy. Tribol T 2013;56(4):555–60.